Published online 4 January 2018 *Nucleic Acids Research, 2018, Vol. 46, No. 5* **2495–2508**
doi: 10.1093/nar/gkx1301

A fungal Argonaute interferes with RNA interference

Quyet Nguyen[1,†], Akihide Iritani[1,†], Shuhei Ohkita[1], Ba V. Vu[1], Kana Yokoya[1], Ai Matsubara[1], Ken-ichi Ikeda[1], Nobuhiro Suzuki[2] and Hitoshi Nakayashiki[1,*]

[1]Laboratory of Cell Function and Structure, Graduate School of Agricultural Science, Kobe University, Nada Kobe 657-8501, Japan and [2]Agrivirology Laboratory, Institute of Plant Science and Resources, Okayama University, Kurashiki, Okayama 710-0046, Japan

Received June 29, 2017; Revised December 13, 2017; Editorial Decision December 15, 2017; Accepted December 19, 2017

ABSTRACT

Small RNA (sRNA)-mediated gene silencing phenomena, exemplified by RNA interference (RNAi), require a unique class of proteins called Argonautes (AGOs). An AGO protein typically forms a protein–sRNA complex that contributes to gene silencing using the loaded sRNA as a specificity determinant. Here, we show that MoAGO2, one of the three AGO genes in the fungus *Pyricularia oryzae* (*Magnaporthe oryzae*) interferes with RNAi. Gene knockout (KO) studies revealed that MoAGO1 and MoAGO3 additively or redundantly played roles in hairpin RNA- and retrotransposon (MAGGY)-triggered RNAi while, surprisingly, the KO mutants of MoAGO2 (Δmoago2) showed elevated levels of gene silencing. Consistently, transcript levels of MAGGY and mycoviruses were drastically reduced in Δmoago2, supporting the idea that MoAGO2 impeded RNAi against the parasitic elements. Deep sequencing analysis revealed that repeat- and mycovirus-derived small interfering RNAs were mainly associated with MoAGO2 and MoAGO3, and their populations were very similar based on their size distribution patterns and positional base preference. Site-directed mutagenesis studies indicated that sRNA binding but not slicer activity of MoAGO2 was essential for the ability to diminish the efficacy of RNAi. Overall, these results suggest a possible interplay between distinct sRNA-mediated gene regulation pathways through a competition for sRNA.

INTRODUCTION

The Argonaute (AGO) protein family is a group of proteins that play key roles in RNA interference (RNAi) and its related pathways. Its members are defined by the presence of conserved domains such as PAZ, MID and PIWI (1). An AGO protein typically forms a protein complex carrying small RNA (sRNA) as a specificity determinant in downstream gene silencing events such as mRNA degradation, translational inhibition and/or heterochromatinization (2,3).

AGO proteins are evolutionarily conserved in the three domains of life. However, the number of AGO genes in each organism differs considerably. For example, there is 1 AGO gene in *Schizosaccharomyces pombe,* while there are 8 in *Homo sapiens* and 27 in *Caenorhabditis elegans* (4), suggesting that AGO-mediated gene regulating pathways could be diverse among organisms. The multiple AGO proteins in an organism mostly have distinct roles in development and/or genome defense, although there are some degrees of redundancy among members. In *Arabidopsis*, both AGO4 and AGO6 are involved in the RNA-directed DNA methylation (RdDM) pathway. However, recent studies have revealed that AGO4 and AGO6 are spatially differentially distributed in the nucleus, and have distinct, but cooperative functions in RdDM. In contrast, AGO1 and AGO10 compete for target microRNA (miRNA) binding (5). The competitive binding for miR166/165 between AGO1 and AGO10 is important for regulating shoot apical meristem development (6). Thus, the relationship between AGO proteins could be independent, cooperative or competitive.

A major biological role of RNAi is to control molecular parasites such as viruses and transposable elements (TEs) in the genome since they are generally regarded to be deleterious to the host cell. However, a genetic mutation caused by TE transposition can also benefit the host. In phytopathogenic fungi, overcoming host resistance often occurs due to a TE-mediated mutation at an avirulence gene that triggers the host defense response. For example, in the rice blast fungus *Pyricularia oryzae* (*Magnaporthe oryzae*), insertion of the Pot3 transposon into the promoter of the avirulence gene, *AVR-Pita*, resulted in gain of virulence toward rice cultivars carrying the corresponding disease resistance gene *Pi-ta* (7). Similarly, TE transposition into the avirulence genes *ACE1* in *P. oryzae* and *AVR2* in *Cladosporium fulvum* resulted in the switch from avirulence to virulence toward resistant rice and tomato cultivars, respectively

*To whom correspondence should be addressed. Tel:/Fax: +81 78 803 5867; Email: hnakaya@kobe-u.ac.jp
† These authors contributed equally to the paper as first authors.

(8,9). These examples clearly show that TEs can contribute to genome plasticity that allows rapid adaptation to a new environment. Thus, TE control in phytopathogenic fungi likely requires a subtle balance between repression and activation.

In the *P. oryzae* genome, we identified three AGO-like genes, MoAGO1, MoAGO2 and MoAGO3. Here we examined the roles of these three AGO genes in RNA silencing pathways of *P. oryzae*. The results indicate that MoAGO1 and MoAGO3 contributed to RNAi but, surprisingly, MoAGO2 interferes with RNAi in *P. oryzae*.

MATERIALS AND METHODS

Construction of gene knockout *P. oryzae* mutants and their gene complementary strains

The wheat-infecting *P. oryzae* isolate, Br48 and its transformants were cultured and maintained as described previously (10). Knockout (KO) mutants of three AGO genes (MoAGO1, MoAGO2, MoAGO3) in *P. oryzae* were constructed by a conventional gene targeting method by homologous recombination. Polymerase chain reaction (PCR) products of upstream and downstream fragments of a targeted gene were cloned into the multiple cloning site of pSP72-hph that carries the Hygromycin resistance gene (hph) cassette (11). The resulting construct was introduced into fungal spheroplasts by a polyethylene glycol-mediated method as described previously (10). For initial screening, colonies PCR were performed with appropriate sets of primers for each gene. Primers used to construct gene disruption vectors and screening were given in Supplementary Table S1. The candidate strains were then examined by Southern blot analysis. Fungal genomic DNA was extracted using Plant Genomic DNA Extraction Miniprep System (Viogene) following the manufacturer's instruction. Southern blot analysis was performed using the DIG DNA Labeling and Detection Kit™ (Roche Applied science). Twenty micrograms of genomic DNA were digested by an appropriate restriction enzyme. The digests were separated by agarose gel electrophoresis and transferred to Hybond N^+ (Amershame biosciense). The hybridization was carried out using PerfectHyb (Sigma-Aldrich) according to the manufacturer's instructions. The positions of DIG-labeled probes used in Southern blot analysis were given in Supplementary Figures S1–3. Genetic complementation of the AGO deletion mutants was performed by introducing the corresponding naïve genomic fragment (MoAGO2) or FLAG-tagged cDNA (MoAGO1, MoAGO3). Genomic DNA fragments containing the MoAGO2 gene with its 5′flanking and 3′flanking regions were amplified with a pair of primers (5′-ggtcacttgcctctttcaaatacc -3′, 5′-acatgcacttccaaaccatcct -3′) using KOD FX Neo (Toyobo), and cloned into pBluescript SK(+).

Plasmid construction

The gene silencing vectors, pSilent2-hyg and pSilent-MG-hyg were constructed by inserting a fragment of the hph gene twice into pSilent2 and once into pSilent-MG, respectively (12,13). pSilent2 is a derivative of pSilent1 carrying a geneticin resistance gene as a selection marker. The hph fragment was PCR-amplified with a pair of primers (5′-ccccagatcttgtttatcggcactttgcat-3′, 5′-ccccagatctgatgttggcgacctcgtatt-3′). cDNA was synthesized from total RNA using Superscript III reverse transcriptase and oligo dT (Thermo Fisher Scientific). A tandem 2× FLAG sequence was attached in frame to 3′ end of *P. oryzae* AGO genes by PCR amplification using cDNA as a template. The PCR products having the full-length AGO sequence attached with 2xFLAG were cloned into the *Sma*I site in pGT carrying the promoter of the glyceraldehyde-3-phosphate dehydrogenase (gpdA) gene, and the terminator of the TrpC gene in *Aspergillus nidulans* (14). The resulting FLAG-tagged MoAGO expression vectors were further modified by replacing the FLAG-tag with a fluorescent protein for cytological observation. Briefly, the vector sequences were amplified by inverse PCR using primers annealing to the upstream and downstream sequences of the FLAG-tag, and joined with a PCR-amplified mCherry or eGFP sequence by in-fusion cloning. The primer sequences used in plasmid construction are shown in Supplementary Table S1.

RNA isolation and quantitative RT-PCR (qRT-PCR)

RNA isolation and cDNA synthesis were performed as described previously with slight modifications (15). Total RNA was isolated from frozen mycelial powder using Sepasol RNA I Super (Nacalai Tesque). One microgram of total RNA was then subjected to cDNA synthesis using the ReverTra Ace qPCR RT Master Mix with gDNA Remover kit (Toyobo). qRT-PCR assay was carried out using FastStart SYBR Green Master (Roche Applied Science) or GeneAce SYBR qPCR Mix α (Nippon Gene) according to the manufacturer's instructions with specific primers for targets and an internal control gene (actin; MGG_03982). The primer sequences are given in Supplementary Table S1. Fluorescence from DNA-SYBR Green complex was monitored by Thermal Cycler Dice Realtime System (Takara Bio) throughout the PCR reaction. The level of target mRNA, relative to the mean of the reference housekeeping gene was calculated by the comparative Ct method. Each experiment was performed with three technical replicates.

Immunoprecipitation, small RNA extraction and high-throughput sequencing

Fungal mycelia were ground with mortar and pestle in liquid nitrogen, and transferred into lysis buffer [50 mM Tris–HCl (pH 7.5), 150 mM NaCl, 1 mM ethylenediaminetetraacetic acid and 0.1% Triton X-100]. After mixing by vortex, cell lysate was collected by centrifugation at 12 000 × *g* for 3min at 4°C, and incubated with Anti-FLAG M2 affinity agarose gel (Sigma-Aldrich) for 3hr on rotation at 4°C. After washing with TBS [50 mM Tris-Cl (pH 7.5), 150 mM NaCl] three times, FLAG-tagged protein was eluted from the agarose gel by incubating with 150 ng/μl FLAG peptide for 30 min at 4°C. The elute was collected by centrifugation at 8000 × *g* for 30 s at 4°C.

For AGO-associated sRNA sequencing, sRNAs were recovered from the FLAG-immunoprecipitates by phenol–

chloroform extraction and ethanol precipitation. For construction of the input library, sRNAs were purified from total RNA by High Pure miRNA isolation kit. Indexed cDNA libraries were prepared with the NEXTflex Small RNA-Seq v3 kit for Illumina (Bioo Scientific) according to the manufacturer's instructions. The cDNA products were purified using Agencourt AMPure XP beads, and enriched with PCR to create the final double stranded cDNA library. The resulting libraries were sequenced on the MiSeq system (Illumina) using single end sequencing with a 75 cycle read length. Sequencing data were analyzed using Genomics workbench software v10.1 (CLCbio). For sRNA mapping, the genome of the *Magnaporthe oryzae* strain 70–15 (release 8.0, http://www.broadinstitute.org/) was used as a reference sequence.

In vitro target RNA cleavage (slicer) assay

Target RNA cleavage assay was performed as described previously (16) with modifications. Slicer assays were performed in a reaction buffer containing 25 mM HEPES-KOH pH 7.5, 5 mM $MgCl_2$, 50 mM KCl, 5 mM dithiothreitol, 2 mM adenosine triphosphate, 0.05 mg/ml bovine serum albumin, 2 U/μl RiboLock RNase Inhibitor (Thermo Scientific). Immunoprecipitated AGO proteins were incubated with FITC-labeled 50 nM target RNA (5′-pGAAGGAGCUUUACAGAGGUUCG GCGUCCUACCAUACGGGG-3′) and control RNA (5′-pAACUCCUCUCUUCGGCGCUAUCCCUCCU GAGCUUACCUUUUAUACAACCG-3′) in the reaction buffer for 1 h at 25°C. After reaction and following phenol:chroloform: isoamyl alcohol (25:24:1) extraction, RNAs were separated on a 12% polyacrylamide TBE–urea denaturing gel and visualized on Typhoon FLA 9500 (GE Healthcare).

To obtain the $MoAGO2^{AEAD}$ and $MoAGO2^{Y619E+K623A}$ mutants, one or two rounds of site-directed mutagenesis were carried out using KOD FX neo polymerase and a pair of primers containing the desired mutation (Supplementary Table S1). After PCR reaction, methylated DNA template was cleaved by *Dpn*I (NEB) at 37°C for 1 h and used for transformation of *Escherichia coli*. Plasmid DNA extracted from selected clones was sequenced to verify the mutation.

Epifluorescence microscopy

Mycelia were viewed under a BZ-9000 epifluorescent microscope (KEYENCE) or a FV1000-KDM confocal laser scanning microscope (Olympus) using a 100 × magnification oil immersion objective. Images were analyzed with BZ-9000 software (KEYENCE) or FLUOVIEW FV1000 MPE software. For visualization of nuclei, cells were stained with Fluoro-KEEPER antifade reagent non-hardening type with DAPI (Nacalai tesque).

RESULTS

MoAGO1 and MoAGO3 are involved in hairpin RNA- and retrotransposon-induced gene silencing while MoAGO2 has a negative impact on gene silencing

We first performed phylogenetic analysis of AGO-like genes in Ascomycota with emphasis on those in Sordariomycetes. AGO-like genes in the genomes of 13 fungal species were employed in the analysis. The number of AGO-like genes varied from 1 (*A. nidulans*, *S. pombe*) to 4 (*Cryphonectria parasitica*, *Gaeumannomyces graminis*) but most of the fungal species examined here possessed three AGO-like genes. Based on their amino acid sequences in the Piwi domain, the AGO genes were clustered into three major groups, which corresponded to the AGO1, AGO2 and AGO3 groups reported previously (62). Three AGO genes in *P. oryzae* were designated MoAGO1 (MGG 14873), MoAGO2 (MGG 13617) and MoAGO3 (MGG 01294) (62). Protein domain analysis using InterPro Scan revealed that all three proteins possessed conserved domains (N-terminal, linker 1, PAZ, linker 2 and Piwi) and conserved amino acid residues (nucleic acid binding site, 5′ RNA guide strand anchoring site and enzymatic active site) (Figure 1B).

To elucidate the roles of MoAGO1, MoAGO2 and MoAGO3 in gene silencing, their KO mutants were constructed using the wheat-infecting *P. oryzae* isolate Br48 (Supplementary Figures S1–3). The resulting KO mutants, Δmoago1, Δmoago2 and Δmoago3, were first subjected to phenotypic analyses, including growth rate, germination, appressorium formation and infectivity. However, all the KO-mutants showed no significant phenotypic changes from the wild-type strain except slightly lower rates of appressorium formation in Δmoago1 and Δmoago3 (Supplementary Figure S4).

We then assessed silencing of the hygromycin resistance (hph) gene in the KO mutants induced by 2 different silencing vectors, pSilent2 and pSilent-MG. pSilent2 produces hairpin RNA of a target gene, and pSilent-MG triggers retrotransposon-induced gene silencing, as it carries the LTR-retrotransposon MAGGY with a cloning site in the 3′ UTR (13,17). In addition to Δmoago1, Δmoago2 and Δmoago3, the wild-type and dicer (modcl2)-KO strains of *P. oryzae* possessing the hph gene were also employed as positive and negative controls, respectively (18).

The levels of hph gene silencing in the resulting transformants were initially evaluated by comparing growth rates on CM media with and without 400 μg/ml Hygromycin B. In the presence of hygromycin, transformants of the wild-type strain with pSilent2-hyg and pSilent-MG-hyg showed an average reduction in growth rate of 45.1 and 42.5%, respectively (Figure 2A), suggesting that the hph gene was significantly silenced either by pSilent2-hyg or by pSilent-MG-hyg. In contrast, in the dicer KO backgrounds, almost no hygromycin-sensitive growth reduction was detected, regardless of the silencing vector, indicating that gene silencing was severely compromised in the dicer mutant. In Δmoago1 and Δmoago3, the rates of hygromycin-sensitive growth reduction by pSilent2-hyg and pSilent-MG-hyg were decreased to approximately 20%. This indicates that gene silencing in Δmoago1 and Δmoago3 was partly impaired at similar levels. Surprisingly, in the Δmoago2 transformants, the rates of hygromycin-sensitive growth reduction were even higher (65.5 and 56.8% by pSilent2-hyg and pSilent-MG-hyg, respectively) than those in the wild-type strain. The enhanced gene silencing in Δmoago2 was restored to the wild-type level by gene complementation (Figure 2A). These results suggest that MoAGO2 negatively affected the

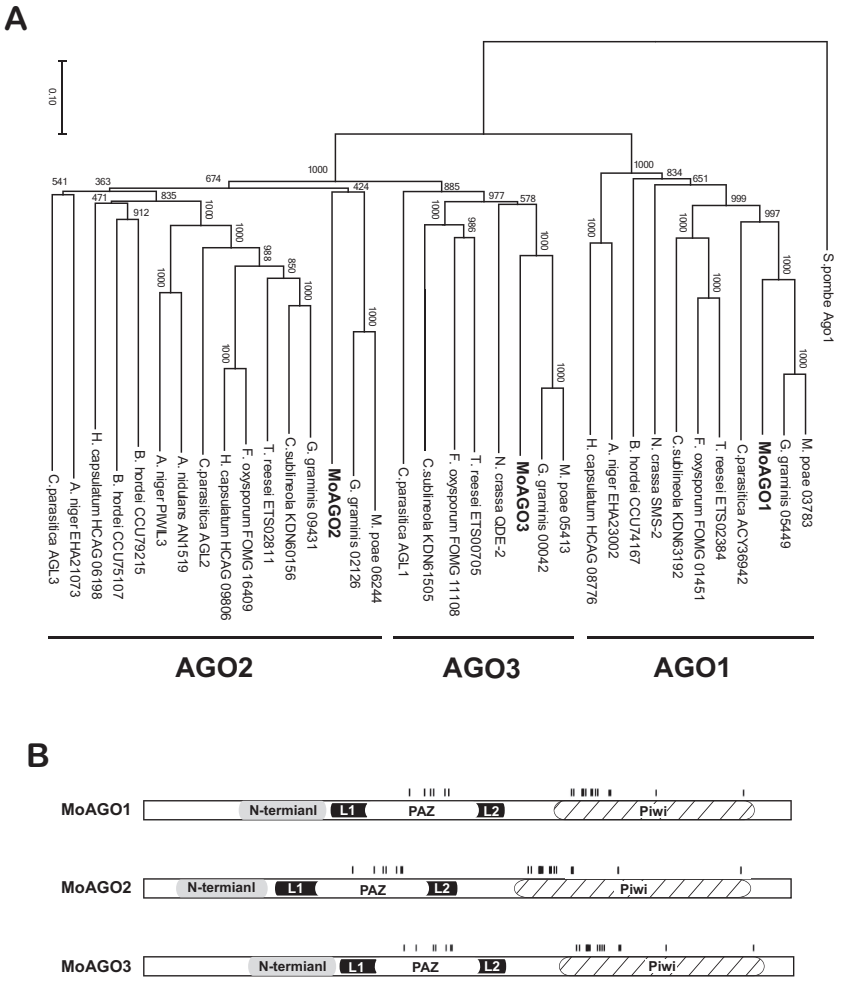

Figure 1. Phylogenetic analysis and schematic representation of 3 AGO genes in *Pyricularia oryzae*. (**A**) A neighbor-joining tree was constructed by alignment of Piwi domain sequences from AGO proteins in Ascomycete fungi. Ago1 in *Schizosaccharomyces pombe* (NP_587782) was used as an outgroup. Bootstrap values are shown from 1000 replicates. Accession numbers of sequences are as follows: *Cryphonectria parasitica* AGL3 (ACY36941), *Aspergillus niger* EHA21073 (CAK38206), *Histoplasma capsulatum* HCAG 06198 (XP_001538593), *Blumeria graminis* f. sp. *hordei* (*B. hordei*) CCU75107 (CCU75107), *B. hordei* CCU79215 (CCU79215), *A. niger* PIWIL3 (XP_001398045), *Aspergillus nidulans* AN1519 (XP_659123), *C. parasitica* AGL2 (ACY36940), *H. capsulatum* HCAG 09806 (XP_001544570), *Fusarium oxysporum* FOMG 16409 (EXK27157), *Trichoderma reesei* ETS02811 (ETS02811), *Colletotrichum sublineola* KDN60156 (KDN60156), *Gaeumannomyces graminis* 09431 (XP_009225543), MoAGO2 (XP_003717504), *G. graminis* 02126 (XP_009218161), *Magnaporthe poae* 06244 (KLU87243), *C. parasitica* AGL1 (ACY36939), *C. sublineola* KDN61505 (KDN61505), *F. oxysporum* FOMG 11108 (EXK33907), *T. reesei* ETS00705 (ETS00705), *Neurospora crassa* QDE-2 (XP_011394903), MoAGO3 (XP_003714217), *G. graminis* 00042 (XP_009216045), *M. poae* 05413 (KLU86399), *H. capsulatum*, HCAG 08776 (XP_001536454), *A. niger* EHA23002 (CAL00657), *B. hordei* CCU74167 (CCU74167), *N. crassa* SMS-2 (XP_958586), *C. sublineola* KDN63192 (KDN63192), *F. oxysporum* FOMG 01451 (XP_018232952), *T. reesei* ETS02384 (ETS02384), *C. parasitica* ACY36942 (ACY36942), MoAGO1 (XP_003716704), *G. graminis* 05449 (XP_009221516) and *M. poae* 03783 (KLU84747). (**B**) Schematic representation of InterPro-predicted protein domains for three AGO genes in *P. oryzae*. Conserved residues for nucleic acid binding site, 5′ RNA guide strand anchoring site and enzymatic active site are indicated as bars. L1, linker 1 domain; L2, linker 2 domain.

efficacy of hph gene silencing induced either by pSilent2-hyg (hairpin RNA) or by pSilent-MG-hyg (retrotransposon).

To verify the results of the hygromycin-sensitivity assay, the expression levels of the hph gene were examined by qRT-PCR in at least five independent transformants of each of the tested strains. Overall, the average levels of hph mRNA in the strains were mostly in accordance with the order of their hygromycin-resistance: Δmoago3 ≈ Δmoago1 > wild-type > Δmoago2 (Figure 2B). These results show that MoAGO1 and MoAGO3 were involved in hairpin RNA- and retrotransposon-induced gene silencing pathways while MoAGO2 had a negative impact on the pathways.

Lack of MoAGO2 enhances gene silencing of the retrotransposon MAGGY and mycoviruses in *P. oryzae*

To examine the effects of the AGO genes on the activity of TEs, we introduced an active copy of the LTR-retrotransposon MAGGY (pMGY70-INT) into the AGO-KO mutants. For each tested strain, 5 to 10 independent transformants with MAGGY were subjected to qRT-PCR analysis. This analysis was performed 2 months after transformation because initial genomic copy numbers of MAGGY in the transformants differed significantly, but the copy numbers averaged with time by autonomous transposition of the element (19). In addition, we also examined

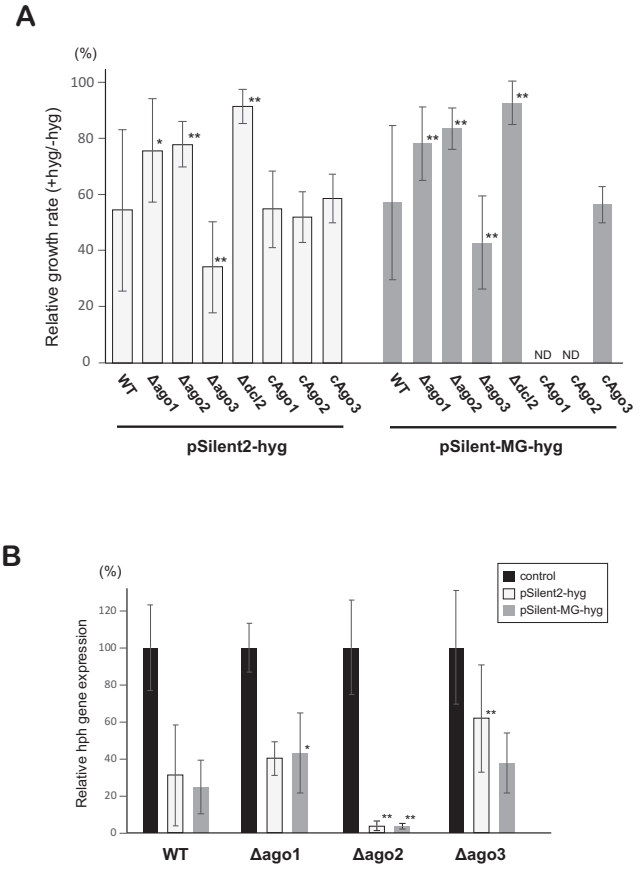

Figure 2. Gene silencing in AGO KO mutants of *Pyricularia oryzae*. (**A**) Transformants with a pSilent2- or pSilent-MG-based vector to knock-down the hygromycin resistance (hph) gene were constructed in various genetic backgrounds as indicated, and cultured on media with or without 400 μg/ml Hygromycin B (hyg). The rate of growth reduction on hyg-containing media relative to that on hyg-less media was calculated for each transformant, and their average was plotted on the graph. cAgo1, cAgo2 and cAgo3 indicate gene complemented strains of Δago1, Δago1 and Δago3, respectively. Asterisks indicate a significant difference from the wild-type (WT) strain (two-tailed *t*-test after angular transformation; $*P < 0.05$; $**P < 0.01$) ND, not determined. (**B**) qRT-PCR analysis of the hph gene in AGO KO mutants transformed with the above-mentioned hph silencing vectors. The parent AGO KO mutants without the silencing vectors were also employed in the analysis to serve as control for normalization. The actin gene (MGG_03982) was used as an internal control. Asterisks indicate a significant difference from WT (two-tailed *t*-test after angular transformation; $*P < 0.05$; $**P < 0.01$).

the transcript level of the endogenous LINE-like element MGL (20,21).

Figure 3A shows relative mRNA quantities of MAGGY and MGL in the AGO-KO mutants and wild-type strain. Compared to the wild-type strain, the levels of MAGGY mRNA were elevated in Δmoago1 and Δmoago3, while the level was significantly decreased in Δmoago2, indicating that MoAGO1 and MoAGO3 play a role in suppressing the accumulation of MAGGY mRNA, whereas MoAGO2 negatively affects MAGGY suppression. In contrast, the transcript level of MGL was not affected significantly by any AGO mutation.

The MAGGY construct (pMGY70-INT) contained an artificial intron within a 3′ LTR (10). RNA-mediated retrotransposition resulted in loss of the intron sequence in progeny copies of MAGGY. Thus, transpositional activity of MAGGY was assessed by the qPCR intron excision assay with sets of PCR primers specific to either the 'exon' junction or the intron internal sequence (Supplementary Figure S5). Figure 3B shows the ratio of the intronless and intron-containing MAGGY DNA fragments in the AGO-KO mutants and wild-type strain. Compared to the wild-type strain, the transposition ratio increased by ∼2-fold in Δmoago3 (Figure 3B), suggesting that MoAGO3 is the major AGO protein responsible for suppression of MAGGY transposition. In contrast, the transposition activity of MAGGY was significantly decreased in Δmoago2. In Δmoago1, the rate of transposition was not significantly different from that in the wild-type strain, although the level of MAGGY mRNA was elevated at levels similar to that in Δmoago3 (Figure 3A and B). This was not surprising because it was previously reported that the rate of MAGGY transposition does not solely depend on the level of MAGGY mRNA in *P. oryzae* (22).

In our previous RNA-seq analysis of the Br48 strain (23), we found two contigs highly homologous to mycoviral RNA-dependent RNA polymerase. Since their amino acid sequences were most closely related to the ourmiavirus-like virus recently reported in *Botrytis cinerea* (24), we tentatively designated them as *P. oryzae* ourmiavirus-like virus 1 and 2 (PoOLV1 and PoOLV2). To assess the effects of the AGO genes on mycoviral multiplication, the levels of PoOLV1 and PoOLV2 RNA were measured by qRT-PCR in the AGO mutants. The PoOLV1 RNA level was ∼2-fold higher in Δmoago3 than in the wild-type strain, suggesting that MoAGO3 is the major AGO protein suppressing PoOLV1 multiplication (Figure 3C). In Δmoago2, the levels of PoOLV1 and PoOLV2 RNA were dramatically decreased to <1/1000 compared to that in the wild-type strain (Figure 3C). Consistently, the level of PoOLV2 accumulation was elevated by the overexpression of MoAGO2. Since the impact of MoAGO2 KO on mycoviral multiplication was much stronger than that on TE transposition and hairpin RNA-induced RNAi, we then asked if the drastic reduction in viral RNA accumulation was due solely to enhanced RNAi using the KO mutant of MoDcl2, the dicer protein responsible for RNAi in vegetative mycelia of *P. oryzae* (18). In the Δmodcl2 background, PoOLV2 RNA accumulation was not affected by KO of the MoAGO2 gene at a statistically significant level. The level of PoOLV1 RNA was significantly decreased in the Δmodcl2/Δmoago2 mutant but only to ∼1/2 compared to the parent Δmodcl2 strain (Figure 3D), indicating that the enhanced silencing of mycoviruses in Δmoago2 was mostly dependent on the MoDcl2-dependent RNAi pathway. Thus, PoOLV1 and PoOLV2 were highly sensitive to RNAi in the absence of MoAGO2. This might be related to the lack of viral coat protein (24) and/or possible lack of an RNA silencing suppressor in this group of mycoviruses. These results overall indicate that MoAGO3 is the major AGO protein responsible for RNAi against parasitic nucleic acids such as TEs and mycoviruses in *P. oryzae*, and that MoAGO2 diminishes the efficacy of RNAi in the wild-type strain.

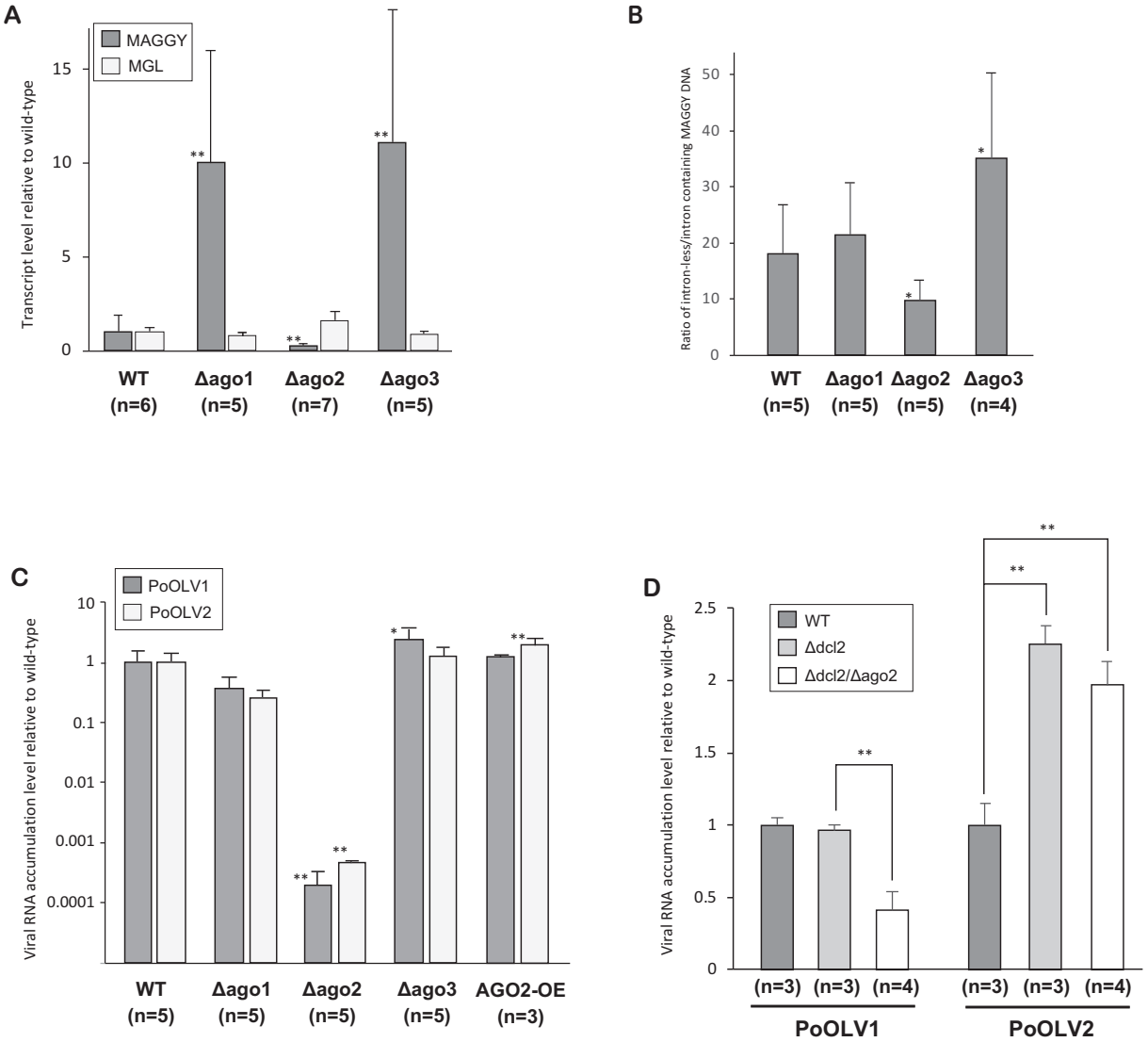

Figure 3. Effects of AGO KO on the activity of TEs and mycoviruses. (**A**) qRT-PCR analysis of TEs (MAGGY and MGL) in AGO KO mutants. The actin gene (MGG_03982) was used as an internal control. Asterisks indicate a significant difference from WT (two-tailed *t*-test; $*P < 0.05$; $**P < 0.01$). (**B**) Intron-excision assay was performed to examine the transposition activity of MAGGY in the AGO mutants. A relative ratio of intron-less or intron-containing MAGGY DNA was measured by qPCR using sets of primers specific to 'exon' junction or intron internal sequences. Asterisks indicate a significant difference from WT (two-tailed *t*-test; $*P < 0.05$; $**P < 0.01$). (**C**) qRT-PCR analysis of mycoviruses (PoOLV1 and PoOLV2) in AGO KO mutants and an AGO2 overexpression (OE) strain. The actin gene was used as an internal control. Asterisks indicate a significant difference from WT (two-tailed *t*-test; $*P < 0.05$; $**P < 0.01$). (**D**) qRT-PCR analysis of mycoviruses (PoOLV1 and PoOLV2) in the wild-type, Δdcl2 and Δdcl2/Δago2 strains. The actin gene was used as an internal control. Asterisks indicate a significant difference (two-tailed *t*-test; $**P < 0.01$).

Alteration of MoAGO1 or MoAGO3 transcription is not the cause of the enhanced RNAi phenotype of Δmoago2

To test the possibility that genetic deletion of the MoAGO2 gene caused complementary upregulation of the other AGO genes, which could result in the enhanced gene silencing of Δmoago2, the transcript levels of the AGO genes in Δmoago2 and its gene complemented strain (cAgo2) were assessed by qRT-PCR. In general, MoAGO3 mRNA was most abundant and MoAGO1 mRNA was rarest in vegetative mycelia of *P. oryzae* (Supplementary Figure S6). No statistically significant upregulation of MoAGO1 or MoAGO3 was detected in Δmoago2 (Supplementary Figure S6). While the average transcript levels of MoAGO1 and MoAGO3 were slightly higher in Δmoago2 than those in the wild-type strain, similar levels of MoAGO1 and MoAGO3 mRNA were observed also in cAgo2 that did not show the enhanced RNAi phenotype (Figure 2A). These results suggest that enhanced RNAi in Δmoago2 was not caused by elevated transcription of the other AGO genes, and thus, that MoAGO2 could negatively regulate the RNAi pathway in *P. oryzae*.

sRNAs associated with AGO proteins in *P. oryzae*

Deep sequencing analysis was performed to characterize sRNAs associated with the three AGO proteins in *P. oryzae*. Each AGO protein was tagged with FLAG at the carboxyl

terminus and expressed in the wild-type strain under the control of the *A. nidulans* gpdA promoter. Using cell extracts from *P. oryzae* mycelia expressing each FLAG-tagged AGO protein (Supplementary Figure S7), sRNAs were isolated from immunoprecipitates with anti-FLAG agarose affinity gel. Since methylguanosine-capped sRNAs in *P. oryzae* were previously reported to range from 16 to 218 nt in length (25), we constructed cDNA libraries using TAP-treated sRNAs without gel size selection. To reduce ligation bias (26), adapters with four randomized bases at the ligation junctions were used in the library construction. As a control to ensure the quality of the cDNA libraries, we also prepared a cDNA library using sRNA collected without FLAG-immunoprecipitation.

Each sample yielded ∼2–5 million sRNA reads sized 15–51 nt after adaptor removal (Table 1). The read mapping to the *P. oryzae* reference genome (70–15 strain) was performed with a cut-off of 80% coverage and 90% identity since we used a wheat infecting strain (Br48) that was closely related to but clustered differently from rice-infecting strains (27). The rates of mapped reads in the cDNA libraries were 93.4–98.2% (Table 1). Most *P. oryzae* sRNAs in the libraries was mapped to rRNA (57.5–87.2%) and tRNA (2.0–15.9%) as reported previously in fungi (28,29) while, surprisingly, only very small portions of sRNAs (0.3–0.2%) were mapped to repeated sequences in this strain (Table 1). Regarding 5′ base preference, A and U were generally preferred (approximately 70% in all AGO-associated sRNA libraries) (Figure 4A). MoAGO2- and MoAGO3-associated sRNAs had a relatively strong preference for 5′-A (38.0%) and 5′-U (42.7%), respectively. It should be noted that the sRNA reads might contain sequences of sRNAs that were just associated with the AGO proteins in addition to ones loaded onto them.

In comparison with the sRNA library constructed without FLAG-immunoprecipitation (input-library), sequences from rRNA, repeats and mycoviruses were enriched in all the AGO-associated sRNA libraries (Table 1), suggesting that rRNA sequences in addition to common RNAi targets (repeats and viruses) were preferentially loaded on AGO proteins in *P. oryzae*. In contrast, sequences from tRNA, snoRNA, intron and intergenic regions were depleted in the AGO-associated sRNA libraries (Table 1). In all the libraries, more than half of the sRNA reads were less than 25 nt (Figure 4B). A strong peak was detected at 19–20 nt in the AGO-associated sRNA libraries that likely contained small interfering RNAs (siRNAs), but it was not detected in the input-library (Figure 4B). Instead, the input-library had a sharp peak at 17 nt that was not detected in the AGO-associated sRNA libraries. Almost all the 17 nt reads were mapped to several tRNA sequences, especially at their 5′ and 3′ ends. This fulfilled the feature of tRNA-derived RNA fragments (tRFs), which was originally reported in human cancer cell lines (30), and also in *P. oryzae* (28).

To characterize sRNA populations in different sizes, rates of 5′-U bases were examined (Figure 4C). Strong preference for 5′-U was observed in AGO-, especially MoAGO2- and MoAGO3-associated sRNA at 19–20 nt. Several other peaks, which in some cases corresponded to peaks in Figure 4B, were also detected (Figure 4C). These peaks were mostly formed due to the presence of certain abundant

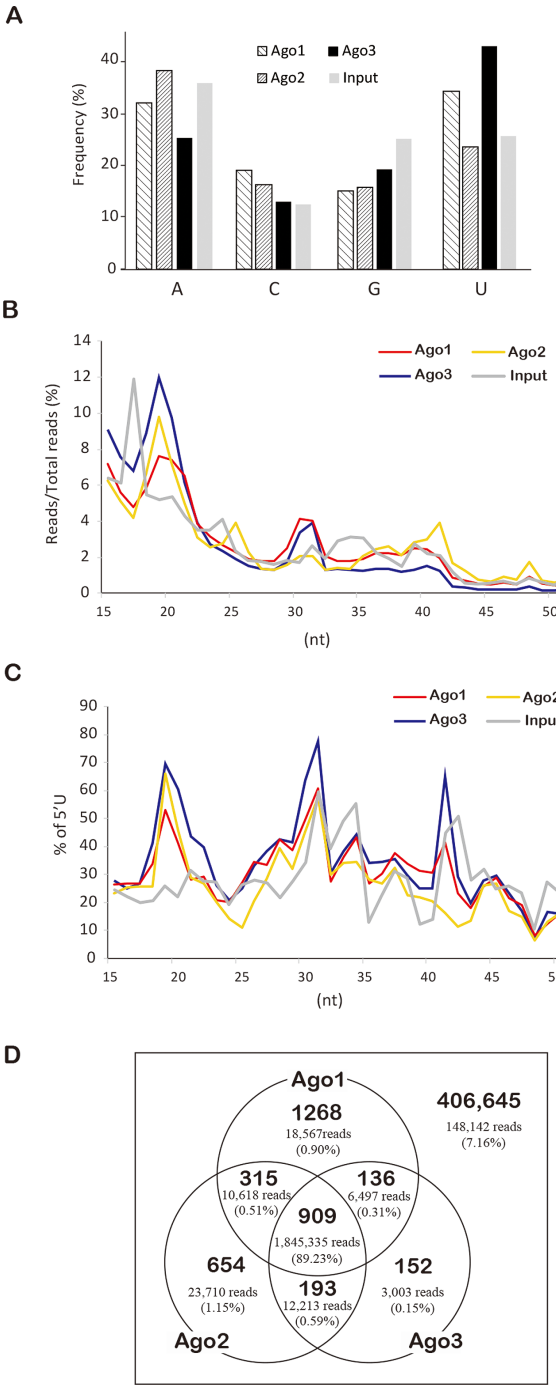

Figure 4. Characteristics of small RNAs (sRNAs) associated with each AGO protein in *Pleomorphomonas oryzae*. (**A**) The relative frequency of each 5′ terminal nucleotide of sRNAs in input RNA (no immunoprecipitation) and those associated with MoAGO1, MoAGO2 and MoAGO3 proteins. (**B**) Size distribution of sRNAs in the input (gray line)-, MoAGO1 (red line)-, MoAGO2 (yellow line)- and MoAGO3 (blue line)-cDNA libraries. (**C**) The relative frequency of 5′-U at each sRNA length in the sRNA cDNA libraries as mentioned in (B). (**D**) Analysis of potential genomic origins of sRNAs associated with each AGO protein in *P. oryzae*. The *P. oryzae* reference genomic sequence was divided into 100-nt blocks and the number of mapped sRNAs in each block was counted. The resulting 410 272 genome blocks were classified based on whether they contained more than 10 mapped RPMs in each library. The number of blocks that met the criteria and the total number of mapped reads in the blocks were plotted for each group of genome blocks.

Table 1. Mapping of sRNA reads to different fractions of the *Pyricularia* (Magnaporthe) oryzae genome

	Total reads	rRNA	tRNA	Exon	Intron	Intergenic	snRNA	snoRNA	Mycovirus	Repeats	Mitochondoria	unmapped
AGO1	2,749,254	2,373,172	127,443	82,397	12,603	34,448	3,382	2305	1,086	2,663	59,597	50,158
		86.32%	4.64%	3.00%	0.46%	1.25%	0.12%	0.08%	0.04%	0.10%	2.17%	1.82%
AGO2	4,494,839	3,918,348	91,453	87,813	20,940	58,557	1,122	5060	3,969	8,673	72,131	226,773
		87.17%	2.03%	1.95%	0.47%	1.30%	0.02%	0.11%	0.09%	0.19%	1.60%	5.05%
AGO3	2,386,599	1,989,805	167,650	66,039	6,918	24,769	2,223	1179	3,923	4,710	37,963	81,420
		83.37%	7.02%	2.77%	0.29%	1.04%	0.09%	0.05%	0.16%	0.20%	1.59%	3.41%
Input	5,292,819	3,042,093	840,342	219,166	203,362	460,740	4,387	41070	154	1,622	126,418	353,465
		57.48%	15.88%	4.14%	3.84%	8.71%	0.08%	0.78%	0.00%	0.03%	2.39%	6.68%

rRNA sequences at the sizes, which could correspond to small rDNA-derived RNAs (srRNAs) reported in other eukaryotes (31,32). The abundant rRNA fragments were almost all derived from transcribed regions of 26S, 18S and 5.8S rRNAs in sense orientation, and often from their partial sequences, forming a stem-like structure as shown in Supplementary Figure S8, or their 5′ and 3′ ends. Table 2 shows the 15 most abundant rRNA fragments that exhibited more than 100-fold enrichment in either of the AGO-associated sRNA libraries relative to the input-library. Interestingly, the abundant rRNA fragments were sometimes preferentially associated with a specific AGO protein in *P. oryzae*. For instance, a peak at 30–31 nt in the MoAGO1- and MoAGO3-libraries was mainly composed of 3′ end fragments of 5.8S rRNA, and a negative peak at 26 nt in the MoAGO2-library was formed due to two major non-5′-U fragments derived from a specific region in 26S rRNA (Table 2). These data clearly indicate that rRNA fragments were specifically associated with AGO protein(s) in *P. oryzae*.

In comparison among the AGO-associated sRNA libraries, tRNA sequences were relatively enriched in the MoAGO3-library and depleted in the MoAGO2-library (Table 1). sRNAs of common RNAi targets (repeats and viruses) were preferentially associated with MoAGO3 and MoAGO2 rather than MoAGO1. To further examine the genomic regions producing sRNAs associated with each AGO protein, the *P. oryzae* reference genomic sequence, which does not include the rRNA cluster and mitochondria sequences, was divided into 100-nt blocks and the number of mapped sRNAs in each block was counted. As a result, 410 272 genome blocks were made, and a total of 2 068 085 reads from the MoAGO1 (662,824 reads)-, MoAGO2 (806,874 reads)- and MoAGO3 (598,387 reads)-libraries were mapped. To reduce background noise, we focused on blocks having more than 10 mapped reads per million reads (RPM) in at least 1 library. Only 3627 (0.88%) of the 410 272 genome blocks met this criteria but included 92.8% of the mapped reads. The 3627 blocks were further classified by the number of RPMs in each AGO library. Figure 4D shows that 909 of the 3627 blocks had more than 10 RPM in every library. Surprisingly, the 909 genome blocks (0.2% of the genome) contained 89.2% of the mapped sRNA reads, indicating that AGO-associated sRNAs were derived from only very limited regions in the genome and that these sRNAs from the 'hot spots' were associated with every AGO protein, indicating that MoAGO1-, MoAGO2- and MoAGO3-associated sRNAs largely shared their genomic origins. However, each AGO protein also had their own mapped sites in the genome (Figure 4D) even though average number of reads per site was significantly lower than the ones at the common 'hot spots'. Notably, MoAGO3 had relatively few specific mapped sites in the genome.

MoAGO2 competes with other *P. oryzae* AGO proteins to bind siRNAs derived from parasitic nucleic acids

To address the negative effects of MoAGO2 on gene silencing, we focused on sRNAs of the TEs (MAGGY and MGL) and mycoviruses (PoOLV1 and PoOLV2) (Figure 3). MAGGY- and MoOLV1-derived sRNAs were preferentially associated with MoAGO2 and MoAGO3 (Figure 5A), suggesting their competitive relationship in binding to those sRNAs. In contrast, the relative rate of MGL-derived sRNAs was much lower in the MoAGO2-library than in the MoAGO3-library, indicating that relatively less MGL-derived sRNAs were associated with MoAGO2. This may partly explain why the absence of MoAGO2 did not significantly affect the transcript level of MGL (Figure 3).

Most of the TE and mycoviral sRNAs were 19–24 nt in size (Figure 5B), suggesting that they are siRNAs functioning in the RNAi pathway. Interestingly, TE and mycoviral siRNAs were peaked at 20 nt while a peak of possible siRNAs was observed at 19 nt in the original AGO-associated sRNA libraries (Figure 4B). An additional weak peak was detected at 24 nt in the TE and mycoviral siRNAs associated with MoAGO2 and MoAGO3 but not MoAGO1, suggesting that the TE and mycoviral siRNA populations associated with MoAGO2 and MoAGO3 were more closely related.

Since MoAGO2- and MoAGO3-associated sRNAs had different preferences for the 5′ base (Figure 4A), we examined 5′ and 3′ base preference in the MoAGO2- and MoAGO3-associated TE and mycoviral siRNAs. The frequencies of 5′-U and 5′-A were, however, similar between the MoAGO2- and MoAGO3-associated siRNA populations as they were for TEs and mycoviruses (Figure 5C). This was also true for 3′ base preference. These results again suggest that similar TE- and mycovirus-derived siRNA populations were competitively loaded on MoAGO2 and MoAGO3, and thus, that the absence of the competitor MoAGO2 could result in enhanced MoAGO3-mediated RNAi against the elements.

sRNA binding but not slicer activity of MoAGO2 is essential for its ability to interfere with RNAi

To gain further insight into the mechanism by which MoAGO2 downmodulates RNAi, we examined if MoAGO2 was an active 'slicer', which is an enzyme that cleaves target RNAs complementary to the bound sRNAs. Crystal structure studies indicated that the PIWI domain contains an RNase H-like fold, where the catalytic

Table 2. Abundant AGO-associated small rDNA-derived RNAs (srRNA) in *Pyricularia oryzae*

				Frequency (%)				Fold enrichment		
Small RNA	Length	Origin	Start Position	AGO1	AGO2	AGO3	Input	AGO1	AGO2	AGO3
CUUGGAUUUAUUGAAGAC UA	20	18S rRNA	908	0.326%	0.150%	0.266%	0.00006%	5760.1	2642.0	4698.6
UGGUUUUUGCGGUUGUCC GA	20	26S rRNA	3007	0.493%	0.399%	0.457%	0.00040%	1241.8	1004.5	1151.0
UCUUGGAUUUAUUGAAGA CUA	21	18S rRNA	907	0.397%	0.223%	0.356%	0.00034%	1167.9	656.5	1045.7
GAUUUAUUGAAGACUA	16	18S rRNA	912	0.355%	0.288%	0.480%	0.00064%	553.3	449.0	747.1
UUGACCCGUUCGGCACCUU	19	18S rRNA	1059	0.324%	0.201%	1.501%	0.00712%	45.5	28.3	210.8
UUGACCCGUUCGGCACCU UA	20	18S rRNA	1059	0.867%	0.564%	3.154%	0.01753%	49.4	32.2	179.9
UGACCCGUUCGGCACCUUA	19	18S rRNA	1060	0.987%	0.542%	2.598%	0.01451%	68.0	37.3	179.1
UGGAUUGUUCACCCACUA	18	26S rRNA	2873	0.291%	0.176%	0.436%	0.00261%	111.5	67.4	167.4
CGGCGGCGGGGGCCCCGG GCAGAGU	25	26S rRNA	1634	0.179%	2.011%	0.185%	0.00123%	146.0	1637.9	150.6
UGACCCGUUCGGCACCUU	18	18S rRNA	1060	0.382%	0.208%	1.320%	0.01181%	32.3	17.6	111.8
CGUUACGAUCUGCUGAGG GUA	21	26S rRNA	3293	1.778%	0.770%	0.681%	0.00786%	226.2	98.0	86.6
CGUUACGAUCUGCUGAGG GU	20	26S rRNA	3293	0.343%	0.136%	0.083%	0.00168%	203.9	80.8	49.1
ACGGCGGCGGGGGCCCCG GGCAGAGU	26	26S rRNA	1633	0.091%	0.866%	0.098%	0.00206%	44.1	420.3	47.5
UGGUAGGACGCCGAACCUC	19	26S rRNA	220	0.904%	4.455%	1.736%	0.04225%	21.4	105.5	41.1
CGGCGGCGGGGGCCCCGG GCAGAG	24	26S rRNA	1634	0.039%	0.648%	0.047%	0.00325%	11.9	199.5	14.5

core of the slicer enzyme is formed by four conserved residues, Asp-Glu-Asp-His/Asp (DEDH/D) (33–35). This signature is detectable in all *P. oryzae* AGO proteins as DEDH in MoAGO1 and DEDD in MoAGO2 and MoAGO3. As a negative control, we made double site-directed mutations (D689A and D763A) in the catalytic core of MoAGO2-FLAG, which was designated MoAGO2 ^{AEAD}.

FLAG-tagged MoAGO3, MoAGO2 and MoAGO2 ^{AEAD}, were purified from the cell extract of *P. oryzae* by immunoprecipitation and subjected to *in vitro* slicer assays using control and target RNAs labeled with FITC. The target RNA had a 40 nt sequence complementary to several abundant endogenous siRNA species derived from 26S rRNA. The control RNA was 50 nt in size and had a target sequence of *Arabidopsis* miR390 (36). By adding FLAG-tagged MoAGO3, a potential slicer in the RNAi pathway of *P. oryzae,* the target RNA was specifically degraded, indicating that MoAGO3 has slicer activity (Figure 6A). Surprisingly, MoAGO2-FLAG also induced specific degradation of the target RNA at a ratio (target/control) similar to that for MoAGO3-FLAG. This suggests that MoAGO2 possessed slicer activity despite its negative impact on RNAi.

We next asked what characteristics of MoAGO2 are required for the ability to impede RNAi. In addition to the slicer mutant MoAGO2 ^{AEAD}, we constructed a site-directed mutant at Y619 and K623, which are supposed to be amino acid residues crucial for sRNA binding (37,38). The resulting MoAGO2 $^{Y619E+K623A}$ mutant showed a drastic reduction in sRNA binding (Supplementary Figure S9). The hygromycin-sensitivity assay was performed after the introduction of MoAGO2-FLAG, MoAGO2^{AEAD}-FLAG and MoAGO2$^{Y619E+K623A}$-FLAG into a Δmoago2 strain showing the hygromycin-hypersensitive phenotype induced by pSilent2-hyg. The results indicated that the enhanced RNAi phenotype of the Δmoago2 strain was restored to the wild-type level by either MoAGO2-FLAG or MoAGO2^{AEAD}-FLAG but not by MoAGO2$^{Y619E+K623A}$-FLAG (Figure 6B). These results suggest that the binding activity to sRNA rather than the slicer activity was important for MoAGO2 to downmodulate RNAi in *P. oryzae*.

MoAGO2 and MoAGO3 are localized to the cytoplasm and cytoplasmic granules

To examine the subcellular localization patterns of MoAGO2 and MoAGO3 in *P. oryzae*, GFP and mCherry were fused to the C-terminus of MoAGO2 and MoAGO3, respectively. The MoAGO2-GFP and MoAGO3-mCherry fusion constructs were simultaneously introduced into the wild-type strain. mCherry and GFP signals were mainly observed in the cytoplasm, and sometimes in cytoplasmic granules (Figure 7). The pattern of the signal localization was consistent with that previously reported for AGO proteins in other organisms (39,40). The AGO proteins in various organisms were often detected in the cytoplasmic granules, called P-bodies (PBs) and/or stress granules (SGs), both of which are evolutionally conserved ribonucleoprotein foci that contain translationally repressed mRNAs together with proteins involved in mRNA degradation and translation repression (41). Thus, the MoAGO2 and MoAGO3-associated cytoplasmic granules might be PBs or SGs in *P. oryzae*.

Signals of MoAGO2 and MoAGO3 were sometimes co-localized but appeared to be independently distributed since the ratio of mCherry and GFP signals differed significantly depending on location in mycelia (Figure 7, merge and Supplementary Figure S10). Especially, some of the cytoplasmic granules consisted of predominantly either MoAGO2 or MoAGO3 even though the others contained both proteins almost evenly. These observations are consistent with our hypothesis that MoAGO2 and MoAGO3 can be competitive in some occasions but have roles in distinct RNA silencing pathways.

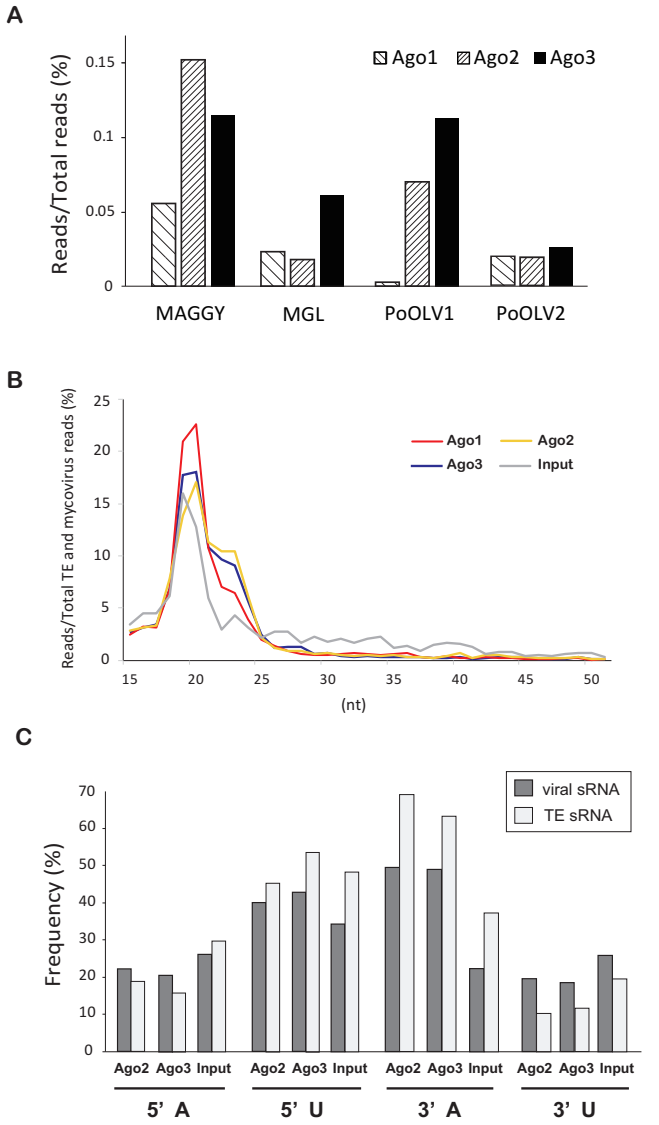

Figure 5. MoAGO2 and MoAGO3 are associated with highly similar siRNA populations derived from TEs and mycoviruses. (**A**) Fractions of siRNAs derived from TEs (MAGGY and MGL) and mycoviruses (PoOLV1 and PoOLV2) in the MoAGO1-, MoAGO2- and MoAGO3-sRNA libraries. (**B**) Size distribution of TE- and mycovirus-derived sRNAs in the input (gray line)-, MoAGO1 (red line)-, MoAGO2 (yellow line)- and MoAGO3 (blue line)-libraries. (**C**) The relative frequency of 5′ and 3′ terminal adenine (A) and thymine (T) of siRNAs derived from TEs and mycoviruses in the input-, MoAGO2- and MoAGO3-sRNA libraries.

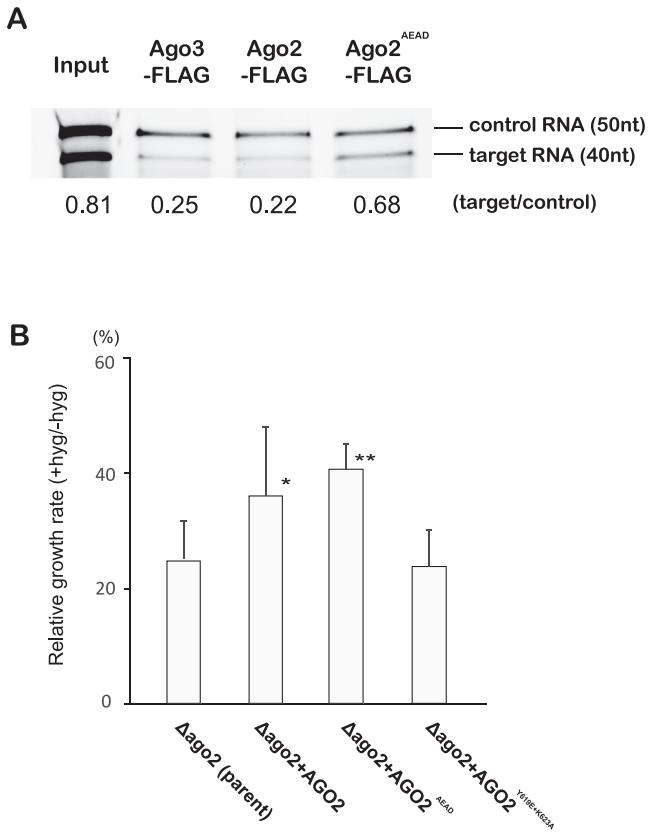

Figure 6. sRNA binding but not slicer activity of MoAGO2 is essential for inhibiting RNAi. (**A**) *In vitro* target RNA cleavage assay. FLAG-tagged MoAGO3, MoAGO2 and MoAGO2^{AEAD} (slicer mutant) were expressed in Δmoago3 cells under the control of a constitutive promoter (*Aspergillus nidulans* gpdA), and purified by immunoprecipitation with anti-FLAG agarose beads. Eluted protein was incubated with FITC-labeled target and control RNAs. Cleaved RNAs were analyzed by a denaturing 12% polyacrylamide gel. The numbers under the bands indicate the intensity of the target bands normalized to the control bands. (**B**) Hygromycin-sensitive growth reduction assay was used to assess the ability of MoAGO2^{AEAD} (slicer mutant) and MoAGO2$^{Y619E+K623A}$ (sRNA binding mutant) to diminish RNAi. A Δmoago2 strain showing a hygromycin-hypersensitive phenotype was used as a parent strain. A plasmid expressing FLAG-tagged MoAGO2, MoAGO2^{AEAD} or MoAGO2$^{Y619E+K623A}$ under the control of the *A. nidulans* gpdA promoter was introduced into the parent strain. Five to ten transformants were cultured on media with or without 400 μg/ml Hygromycin B (hyg). The rate of growth reduction on hyg-containing media relative to that on hyg-less media was calculated for each transformant, and their average was plotted on the graph. Asterisks indicate a significant difference from the parent strain (two-tailed t-test after angular transformation; $*P < 0.05$; $**P < 0.01$).

DISCUSSION

MoAGO2 negatively affects the RNAi (siRNA) pathway in *P. oryzae*

In eukaryotes, AGO proteins are involved in a variety of biological processes using sRNA as a specificity determinant. Predominant AGO-associated sRNA species include miRNA, siRNA, Piwi-interacting RNA (piRNA) and heterochromatic siRNAs (hc-siRNAs). AGO–sRNA complexes are often called RNA-induced silencing complexes (RISCs), since these complexes generally regulate gene expression negatively. For instance, miRNA-, siRNA- and piRNA-RISCs function in various types of post-transcriptional gene silencing, whereas hc-siRNA-RISCs mediate transcriptional gene silencing by inducing DNA methylation (42,43).

In filamentous fungi, mechanisms of RNA silencing have been extensively studied in *Neurospora crassa*, leading to identification of two major RNA-silencing pathways, namely quelling and meiotic silencing by unpaired DNA (MSUD) (44,45). Quelling is a vegetative RNA silencing while MSUD operates as meiotic silencing. *Neurospora* AGO genes Qde-2 and Sms-2 are involved in the quelling and MSUD pathways, respectively (44). Phylogenetic anal-

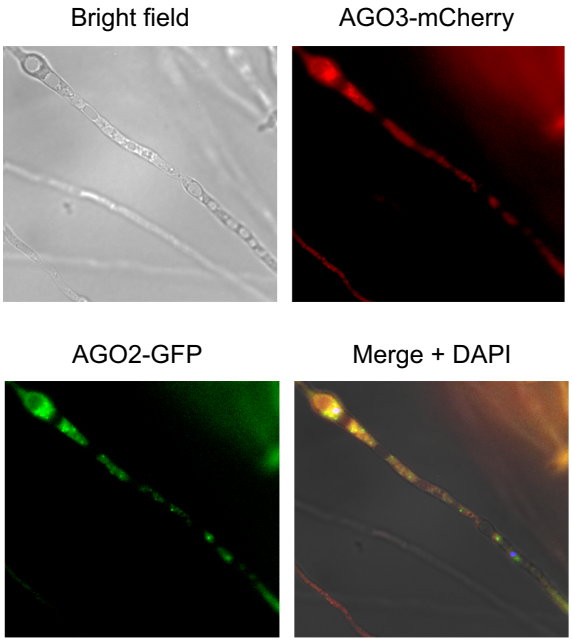

Figure 7. MoAGO2 and MoAGO3 are localized in the cytoplasm and cytoplasmic granules. GFP-tagged MoAGO2 and mCherry-tagged MoAGO3 were co-expressed in the wild-type *Pyricularia oryzae* cells. Images were captured using the KEYENCE BZ-9000 epifluorescent microscope and analysed using BZ-9000 software. Nuclei were visualized by DAPI staining.

ysis revealed that MoAGO3 and MoAGO1 were homologous to Qde-2 and Sms-2, respectively, but no counterpart of MoAGO2 was found in *N. crassa*.

In this study, the deletion of MoAGO2, one of the three *P. oryzae* AGO proteins, resulted in even higher efficiency of gene silencing than that in the wild-type when triggered by hairpin RNA, an LTR-retrotransposon, or mycoviruses. Since these triggers are typical targets of the RNAi (siRNA-mediated) pathway, MoAGO2 appeared to be a negative regulator of the pathway and thus a unique AGO protein. A possible related phenomenon is 'sequestration', which was reported as a competitive interaction between AGO proteins in plants, where an AGO protein acted as a decoy of a specific miRNA to sequester it from binding to the competitive AGO protein (6,46). For instance, *Arabidopsis* AGO10 competed with AGO1 for binding to miR165/166. This competitive binding diminished miR165/166-directed cleavage of the target HD-ZIP III mRNA by AGO1, and consequently regulated normal shoot apical meristem development (6). Interestingly, like MoAGO2, *Arabidopsis* AGO10 has slicer activity. However, the miRNA binding ability of AGO10 but not its slicer activity was required for sequestration (6). Similar to AGO10 in *Arabidopsis*, rice AGO18 preferentially associated with miR168 to sequester it from targeting rice AGO1 that was essential for antiviral RNAi (46). The expression of AGO18 was induced by viral infection, and subsequently led to the up-regulation of AGO1. Thus, AGO18 contributed to broad-spectrum virus resistance in rice by sequestering miR168. Our data suggested that MoAGO2 could interfere with RNAi in *P. oryzae* likely in a manner similar to that of sequestration in plants. However, competitive interaction between MoAGO2 and MoAGO3 was not limited to specific sRNA species but rather included a broad range of siRNAs derived from artificial hairpin RNA, TEs and mycoviruses.

The competitive relationship between MoAGO2 and MoAGO3 may be explained as a conflict between two distinct sRNA-mediated gene regulation pathways. In plants, siRNAs derived from various sources including hairpin RNA, TEs and viruses function in the RdDM pathway as well as in the RNAi (mRNA degradation) pathway (47,48) even though the classes of siRNAs involved in the pathways can be different at least partly. In *P. oryzae*, while no sRNA-related pathways other than RNAi have been so far identified, it may be possible that MoAGO2 is involved in RdDM or a yet unknown pathway that uses siRNA as a specificity determinant, leading to a competition for siRNA against RNAi.

Alternatively, MoAGO2 may not function as an active AGO but may act as a modulator of RNAi. Since several fungal species such as *N. crassa* do not possess an AGO2 family protein, this class of AGO genes may not play an essential role in fungal growth and development. Actually, Δmoago2 did not show any apparent phenotype other than enhanced gene silencing in this study (Supplementary Figure S4). As stated above, in pathogenic microorganisms, TEs sometimes benefit hosts by providing genetic alterations to adapt a new environmental condition, especially to adapt a new host. It has been observed in *P. oryzae* that a new strain overcoming host disease resistance occurred by a TE-mediated genetic change. However, in Br48, the wheat-infecting *P. oryzae* strain used in this study, the activity of TEs is extremely low likely due to repeat-induced point mutation (RIP). RIP is a process that detects DNA duplications and causes genetic changes (C:G to T:A transitions) in duplicated sequences during the sexual phase of the life cycle (49,50). Therefore, RIP can eliminate the activity of TEs permanently from the genome. Unlike common rice-infecting *P. oryzae* strains that lack the sexual phase, Br48 is highly fertile and possesses RIP as a currently active process (51). In our previous RNA-seq analysis, very few TEs were transcriptionally active (23). This was also indicated in this study, as the portion of TE-derived sRNAs was extremely low compared to that previously reported in rice-infecting *P. oryzae* strains (Table 1; (28,52)). Considering recent findings on the contributions of TEs to the genome plasticity and evolution in fungi, MoAGO2 might become a very unique modulator for maintaining TEs moderately active to generate new genetic variations in this phytopathogenic fungus.

rRNA-related sRNAs in *P. oryzae*

Eukaryotic rRNAs such as 28S, 18S and 5.8S rRNAs are abundantly transcribed from the rDNA clusters, and make up ∼80% of the total RNA in the cytoplasm (53). In deep sequencing of sRNA, sRNAs mapped to the rRNA clusters were often omitted from detailed analysis, as they could be degradation products of abundant RNA. Surprisingly, in this study, the large majority of the AGO-associated sRNA in Br48 was derived from rRNA. This unusually high ratio of rRNA sequences in the libraries was thought to be,

at least partly, due to very low levels of repeat-derived sRNAs in this strain, which usually account for most sRNAs in eukaryotic cells. Nevertheless, our data clearly demonstrate that rRNA-derived sRNAs were preferentially associated with the AGO proteins in *P. oryzae*. Notably, some of them showed more than 1000-fold enrichment in the AGO-associated sRNA library compared to the input-library (Table 2). Thus, the association is highly specific, and not likely to depend on random degradation of rRNA.

Such abundant rRNA fragments (srRNAs) have recently been reported in mammals and plants (31,32). The characteristics of the rRNA fragments identified in this study were well matched to those of srRNAs: (i) derived from mature rRNA molecules in sense orientation, (ii) often mapped to 5′ and 3′ ends of rRNAs and internal sequences that potentially form a stem-like structure. Thus, srRNAs seem to be conserved in a wide range of eukaryotes including mammals, plants and fungi. In the fungus *N. crassa*, another type of rRNA-related sRNA, designated QDE2-interacting small RNA (qiRNA), was previously identified (54). qiRNA was induced in response to DNA damage, and played a role in suppressing protein synthesis after DNA damage. However, unlike srRNAs, qiRNAs were produced from non-transcribed regions as well as transcribed regions in the rDNA cluster almost equally in both sense and antisense orientations (54). These characteristics of qiRNA appear to be more closely related to DNA double strand break-induced small RNA rather than srRNAs (55).

The biological roles of srRNAs are yet to be elucidated. In mammals, overexpression or inhibition of several srRNA species led to altered expression levels of genes involved in biological processes such as glucose metabolism and cell division, but did not significantly change rRNA levels (31). In this context, human AGO2 has been recently demonstrated to bind to nuclear nascent rRNA in a miRNA-mediated manner (56). PAR-CLIP-seq followed by RIP-qPCR verification identified 479 possible AGO2 binding sites in 45S RNA, the precursor RNA that is processed into the 18S, 5.8S and 28S rRNAs. Knockdown of AGO2 resulted in a slight, but statistically significant increase in the overall rRNA synthesis (56). In addition, DICER has been shown to reside within the nucleolus and associate with rDNA regions in mammals (57). Thus, RNAi machinery seems to play roles in various rRNA-related gene regulations in a wide range of eukaryotes, with possible involvement of srRNAs.

5′ terminal bases of sRNAs are unlikely to be determinants of their association with a specific AGO protein in *P. oryzae*

In *Arabidopsis*, it was proposed that sorting of sRNAs for specific AGO loading was directed by recognition of their 5′ nucleotides (58–60). For example, *Arabidopsis* AGO1 preferentially binds miRNAs with a 5′-U, whereas AGO2 has a bias toward siRNAs with a 5′-A (58–60). In our study, while a strong bias to 5′-U was observed with siRNAs from TEs and mycoviruses and those siRNAs were preferentially associated with MoAGO2 and MoAGO3, a similar strong bias toward 5′-U was also observed in MoAGO1-associated TE and virus-derived siRNAs. In addition, such a strong 5′-U preference was not observed in sRNAs at different lengths (Figure 4B). Consistently, the 5′ base of the abundant srRNAs specifically associated with a certain AGO protein was not always constant (Table 2). Overall, it was unlikely that 5′ terminal bases of sRNAs determined a specific association with an AGO protein in *P. oryzae*. The strong 5′-U preference detected in AGO-associated siRNAs derived from TEs and mycoviruses might be due to the mechanism of their biogenesis such as the ping-pong model proposed for piRNA biogenesis (61).

DATA AVAILABILITY

The small RNA sequencing data have been deposited in the DDBJ Sequence Read Archive under the accession, DRA005932.

SUPPLEMENTARY DATA

Supplementary Data are available at NAR Online.

ACKNOWLEDGEMENT

We would like thank Hiro-oki Iwakawa (University of Tokyo) for critical reading of the manuscript, and for the gifts of miR390 RNA and its target (pGL3-basic) as well as his technical advice for slicer assay.

FUNDING

Japan Society for the Promotion of Science, Grant-in-Aid for Scientific Research (A) and (B) [#25252011, #25292028, #16H04883]. Funding for open access charge: Japan Society for the Promotion of Science [#16H04883].
Conflict of interest statement. None declared.

REFERENCES

1. Tolia,N.H. and Joshua-Tor,L. (2007) Slicer and the argonautes. *Nat. Chem. Boil.*, **3**, 36–43.
2. Moazed,D. (2009) Small RNAs in transcriptional gene silencing and genome defence. *Nature*, **457**, 413–420.
3. Siomi,M.C., Sato,K., Pezic,D. and Aravin,A.A. (2011) PIWI-interacting small RNAs: the vanguard of genome defence. *Nat. Rev. Mol. Cell. Biol.*, **12**, 246–258.
4. Hock,J. and Meister,G. (2008) The Argonaute protein family. *Genome Biol.*, **9**, 210.
5. Mallory,A.C., Hinze,A., Tucker,M.R., Bouche,N., Gasciolli,V., Elmayan,T., Lauressergues,D., Jauvion,V., Vaucheret,H. and Laux,T. (2009) Redundant and specific roles of the ARGONAUTE proteins AGO1 and ZLL in development and small RNA-directed gene silencing. *PLoS Genet.*, **5**, e1000646.
6. Zhu,H., Hu,F., Wang,R., Zhou,X., Sze,S.H., Liou,L.W., Barefoot,A., Dickman,M. and Zhang,X. (2011) Arabidopsis Argonaute10 specifically sequesters miR166/165 to regulate shoot apical meristem development. *Cell*, **145**, 242–256.
7. Kang,S., Lebrun,M.H., Farrall,L. and Valent,B. (2001) Gain of virulence caused by insertion of a Pot3 transposon in a *Magnaporthe grisea* avirulence gene. *Mol. Plant Microbe Interact.*, **14**, 671–674.
8. Luderer,R., Takken,F.L., de Wit,P.J. and Joosten,M.H. (2002) *Cladosporium fulvum* overcomes Cf-2-mediated resistance by producing truncated AVR2 elicitor proteins. *Mol. Microbiol.*, **45**, 875–884.
9. Fudal,I., Bohnert,H.U., Tharreau,D. and Lebrun,M.H. (2005) Transposition of MINE, a composite retrotransposon, in the avirulence gene ACE1 of the rice blast fungus *Magnaporthe grisea*. *Fungal Genet. Biol.*, **42**, 761–772.

10. Nakayashiki,H., Kiyotomi,K., Tosa,Y. and Mayama,S. (1999) Transposition of the retrotransposon MAGGY in heterologous species of filamentous fungi. *Genetics*, **153**, 693–703.
11. Morita,Y., Hyon,G.S., Hosogi,N., Miyata,N., Nakayashiki,H., Muranaka,Y., Inada,N., Park,P. and Ikeda,K. (2013) Appressorium-localized NADPH oxidase B is essential for aggressiveness and pathogenicity in the host-specific, toxin-producing fungus *Alternaria alternata* Japanese pear pathotype. *Mol. Plant Pathol.*, **14**, 365–378.
12. Nakayashiki,H., Hanada,S., Nguyen,B.Q., Kadotani,N., Tosa,Y. and Mayama,S. (2005) RNA silencing as a tool for exploring gene function in ascomycete fungi. *Fungal Genet. Biol.*, **42**, 275–283.
13. Vu,V.B., Takino,M., Murata,T. and Nakayashiki,H. (2011) Novel vectors for retrotransposon-induced gene silencing in *Magnaporthe oryzae*. *J. Gen. Plant Pathol.*, **77**, 147–151.
14. Kadotani,N., Murata,T., Quoc,N.B., Adachi,Y. and Nakayashiki,H. (2008) Transcriptional control and protein specialization have roles in the functional diversification of two dicer-like proteins in *Magnaporthe oryzae*. *Genetics*, **180**, 1245–1249.
15. Nguyen,Q.B., Itoh,K., Vu,V.B., Tosa,Y. and Nakayashiki,H. (2011) Simultaneous silencing of endo-beta-1,4 xylanase genes reveals their roles in the virulence of *Magnaporthe oryzae*. *Mol. Microbiol.*, **81**, 1008–1019.
16. Park,M.S., Phan,H.D., Busch,F., Hinckley,S.H., Brackbill,J.A., Wysocki,V.H. and Nakanishi,K. (2017) Human Argonaute3 has slicer activity. *Nucleic Acids Res.*, **45**, 11867–11877.
17. Farman,M.L., Tosa,Y., Nitta,N. and Leong,S.A. (1996) MAGGY, a retrotransposon in the genome of the rice blast fungus *Magnaporthe grisea*. *Mol. Gen. Genet.*, **251**, 665–674.
18. Kadotani,N., Nakayashiki,H., Tosa,Y. and Mayama,S. (2004) One of the two dicer-like proteins in the filamentous fungi *Magnaporthe oryzae* genome is responsible for hairpin RNA-triggered RNA silencing and related siRNA accumulation. *J. Biol. Chem.*, **279**, 44467–44474.
19. Nakayashiki,H., Ikeda,K., Hashimoto,Y., Tosa,Y. and Mayama,S. (2001) Methylation is not the main force repressing the retrotransposon MAGGY in *Magnaporthe grisea*. *Nucleic Acids Res.*, **29**, 278–284.
20. Hamer,J., Farrall,L., Orbach,M., Valent,B. and Chumley,F. (1989) Host species-specific conservation of a family of repeated DNA sequences in the genome of a fungal plant pathogen. *Proc. Natl. Acad. Sci. U.S.A.*, **86**, 9981–9985.
21. Kachroo,P., Ahuja,M., Leong,S.A. and Chattoo,B.B. (1997) Organisation and molecular analysis of repeated DNA sequences in the rice blast fungus *Magnaporthe grisea*. *Curr. Genet.*, **31**, 361–369.
22. Murata,T., Kadotani,N., Yamaguchi,M., Tosa,Y., Mayama,S. and Nakayashiki,H. (2007) siRNA-dependent and -independent post-transcriptional cosuppression of the LTR-retrotransposon MAGGY in the phytopathogenic fungus *Magnaporthe oryzae*. *Nucleic Acids Res.*, **35**, 5987–5994.
23. Pham,K.T., Inoue,Y., Vu,B.V., Nguyen,H.H., Nakayashiki,T., Ikeda,K. and Nakayashiki,H. (2015) MoSET1 (Histone H3K4 Methyltransferase in *Magnaporthe oryzae*) regulates global gene expression during Infection-related morphogenesis. *PLoS Genet*., **11**, e1005385.
24. Donaire,L., Rozas,J. and Ayllon,M.A. (2016) Molecular characterization of Botrytis ourmia-like virus, a mycovirus close to the plant pathogenic genus Ourmiavirus. *Virology*, **489**, 158–164.
25. Gowda,M., Venu,R.C., Raghupathy,M.B., Nobuta,K., Li,H., Wing,R., Stahlberg,E., Couglan,S., Haudenschild,C.D., Dean,R. *et al.* (2006) Deep and comparative analysis of the mycelium and appressorium transcriptomes of *Magnaporthe grisea* using MPSS, RL-SAGE, and oligoarray methods. *BMC Genomics*, **7**, 310.
26. Jayaprakash,A.D., Jabado,O., Brown,B.D. and Sachidanandam,R. (2011) Identification and remediation of biases in the activity of RNA ligases in small-RNA deep sequencing. *Nucleic Acids Res.*, **39**, e141.
27. Murata,N., Aoki,T., Kusaba,M., Tosa,Y. and Chuma,I. (2014) Various species of *Pyricularia* constitute a robust clade distinct from *Magnaporthesalvinii* and its relatives in Magnaporthaceae. *J. Gen. Plant Pathol.*, **80**, 66–72.
28. Nunes,C.C., Gowda,M., Sailsbery,J., Xue,M., Chen,F., Brown,D.E., Oh,Y., Mitchell,T.K. and Dean,R.A. (2011) Diverse and tissue-enriched small RNAs in the plant pathogenic fungus, Magnaporthe oryzae. *BMC Genomics*, **12**, 288.
29. Lee,H.C., Li,L., Gu,W., Xue,Z., Crosthwaite,S.K., Pertsemlidis,A., Lewis,Z.A., Freitag,M., Selker,E.U., Mello,C.C. *et al.* (2010) Diverse pathways generate microRNA-like RNAs and Dicer-independent small interfering RNAs in fungi. *Mol. Cell*, **38**, 803–814.
30. Lee,Y.S., Shibata,Y., Malhotra,A. and Dutta,A. (2009) A novel class of small RNAs: tRNA-derived RNA fragments (tRFs). *Genes Dev.*, **23**, 2639–2649.
31. Wei,H., Zhou,B., Zhang,F., Tu,Y., Hu,Y., Zhang,B. and Zhai,Q. (2013) Profiling and identification of small rDNA-derived RNAs and their potential biological functions. *PLoS One*, **8**, e56842.
32. Asha,S. and Soniya,E.V. (2017) The sRNAome mining revealed existence of unique signature small RNAs derived from 5.8SrRNA from *Piper nigrum* and other plant lineages. *Sci. Rep.*, **7**, 41052.
33. Song,J.J., Smith,S.K., Hannon,G.J. and Joshua-Tor,L. (2004) Crystal structure of Argonaute and its implications for RISC slicer activity. *Science*, **305**, 1434–1437.
34. Rivas,F.V., Tolia,N.H., Song,J.J., Aragon,J.P., Liu,J., Hannon,G.J. and Joshua-Tor,L. (2005) Purified Argonaute2 and an siRNA form recombinant human RISC. *Nat. Struct. Mol. Biol.*, **12**, 340–349.
35. Nakanishi,K., Weinberg,D.E., Bartel,D.P. and Patel,D.J. (2012) Structure of yeast Argonaute with guide RNA. *Nature*, **486**, 368–374.
36. Endo,Y., Iwakawa,H.O. and Tomari,Y. (2013) Arabidopsis ARGONAUTE7 selects miR390 through multiple checkpoints during RISC assembly. *EMBO Rep.*, **14**, 652–658.
37. Rüdel,S., Wang,Y., Lenobel,R., Körner,R., Hsiao,H.H., Urlaub,H., Patel,D. and Meister,G. (2011) Phosphorylation of human Argonaute proteins affects small RNA binding. *Nucleic Acids Res.*, **39**, 2330–2343.
38. Schirle,N.T. and MacRae,I.J. (2012) The crystal structure of human Argonaute2. *Science*, **336**, 1037–1040.
39. Liu,J., Valencia-Sanchez,M.A., Hannon,G.J. and Parker,R. (2005) MicroRNA-dependent localization of targeted mRNAs to mammalian P bodies. *Nat. Cell Biol.*, **7**, 719–723.
40. Leung,A.K., Calabrese,J.M. and Sharp,P.A. (2006) Quantitative analysis of Argonaute protein reveals microRNA-dependent localization to stress granules. *Proc. Natl. Acad. Sci. U.S.A.*, **103**, 18125–18130.
41. Parker,R. and Sheth,U. (2007) P bodies and the control of mRNA translation and degradation. *Mol. Cell*, **25**, 635–646.
42. Borges,F. and Martienssen,R.A. (2015) The expanding world of small RNAs in plants. *Nat. Rev. Mol. Cell Biol.*, **16**, 727–741.
43. Fang,X. and Qi,Y. (2016) RNAi in plants: an argonaute-centered view. *Plant Cell*, **28**, 272–285.
44. Nakayashiki,H. (2005) RNA silencing in fungi: mechanisms and applications. *FEBS Lett.*, **579**, 5950–5957.
45. Li,L., Chang,S.S. and Liu,Y. (2010) RNA interference pathways in filamentous fungi. *Cell Mol. Life Sci.*, **67**, 3849–3863.
46. Wu,J., Yang,Z., Wang,Y., Zheng,L., Ye,R., Ji,Y., Zhao,S., Ji,S., Liu,R., Xu,L. *et al.* (2015) Viral-inducible Argonaute18 confers broad-spectrum virus resistance in rice by sequestering a host microRNA. *Elife*, **4**, e05733.
47. Mette,M.F., Aufsatz,W., van der Winden,J., Matzke,M.A. and Matzke,A.J. (2000) Transcriptional silencing and promoter methylation triggered by double-stranded RNA. *EMBO J.*, **19**, 5194–5201.
48. Bond,D.M. and Baulcombe,D.C. (2015) Epigenetic transitions leading to heritable, RNA-mediated de novo silencing in *Arabidopsis thaliana*. *Proc. Natl. Acad. Sci. U.S.A.*, **112**, 917–922.
49. Selker,E.U., Cambareri,E.B., Jensen,B.C. and Haack,K.R. (1987) Rearrangement of duplicated DNA in specialized cells of *Neurospora*. *Cell*, **51**, 741–752.
50. Cambareri,E.B., Jensen,B.C., Schabtach,E. and Selker,E.U. (1989) Repeat-induced G-C to A-T mutations in *Neurospora*. *Science*, **244**, 1571–1575.
51. Ikeda,K., Nakayashiki,H., Kataoka,T., Tamba,H., Hashimoto,Y., Tosa,Y. and Mayama,S. (2002) Repeat-induced point mutation (RIP) in *Magnaporthe grisea*: implications for its sexual cycle in the natural field context. *Mol. Microbiol.*, **45**, 1355–1364.
52. Raman,V., Simon,S.A., Romag,A., Demirci,F., Mathioni,S.M., Zhai,J., Meyers,B.C. and Donofrio,N.M. (2013) Physiological stressors and invasive plant infections alter the small RNA transcriptome of the rice blast fungus, Magnaporthe oryzae. *BMC Genomics*, **14**, 326.

53. Kampers,T., Friedhoff,P., Biernat,J., Mandelkow,E. and Mandelkow,E. (1996) RNA stimulates aggregation of microtubule-associated protein tau into Alzheimer-like paired helical filaments. *FEBS Lett.*, **399**, 344–349.
54. Lee,H.C., Chang,S.S., Choudhary,S., Aalto,A.P., Maiti,M., Bamford,D.H. and Liu,Y. (2009) qiRNA is a new type of small interfering RNA induced by DNA damage. *Nature*, **459**, 274–277.
55. Wei,W., Ba,Z., Gao,M., Wu,Y., Ma,Y., Amiard,S., White,C.I., Rendtlew Danielsen,J.M., Yang,Y.G. and Qi,Y. (2012) A role for small RNAs in DNA double-strand break repair. *Cell*, **149**, 101–112.
56. Atwood,B.L., Woolnough,J.L., Lefevre,G.M., Saint Just Ribeiro,M., Felsenfeld,G. and Giles,K.E. (2016) Human Argonaute 2 is tethered to ribosomal RNA through microRNA interactions. *J. Biol. Chem.*, **291**, 17919–17928.
57. Sinkkonen,L., Hugenschmidt,T., Filipowicz,W. and Svoboda,P. (2010) Dicer is associated with ribosomal DNA chromatin in mammalian cells. *PLoS One*, **5**, e12175.
58. Mi,S., Cai,T., Hu,Y., Chen,Y., Hodges,E., Ni,F., Wu,L., Li,S., Zhou,H., Long,C. *et al.* (2008) Sorting of small RNAs into Arabidopsis argonaute complexes is directed by the 5′ terminal nucleotide. *Cell*, **133**, 116–127.
59. Montgomery,T.A., Yoo,S.J., Fahlgren,N., Gilbert,S.D., Howell,M.D., Sullivan,C.M., Alexander,A., Nguyen,G., Allen,E., Ahn,J.H. *et al.* (2008) AGO1-miR173 complex initiates phased siRNA formation in plants. *Proc. Natl. Acad. Sci. U.S.A.*, **105**, 20055–20062.
60. Takeda,A., Iwasaki,S., Watanabe,T., Utsumi,M. and Watanabe,Y. (2008) The mechanism selecting the guide strand from small RNA duplexes is different among argonaute proteins. *Plant Cell Physiol.*, **49**, 493–500.
61. Brennecke,J., Aravin,A.A., Stark,A., Dus,M., Kellis,M., Sachidanandam,R. and Hannon,G.J. (2007) Discrete small RNA-generating loci as master regulators of transposon activity in *Drosophila*. *Cell*, **128**, 1089–1103.
62. Raman,V., Simon,S.A., Demirci,F., Nakano,M., Meyers,B.C. and Donofrio,N.M. (2017) Small RNA functions are required for growth and development of *magnaporthe oryzae*. *Mol. Plant Microbe Interact.*, **30**, 517–530.